Received: Added at production | Revised: Added at production | Accepted: Added at production

DOI: xxx/xxxx

RESEARCH ARTICLE

Abiotic ribonucleoside formation in aqueous microdroplets: mechanistic exploration, acidity, and electric field effects

Maciej Piejko[1] | **Javier E. Alfonso-Ramos**[2] | **Joseph Moran**[1,3] | **Thijs Stuyver**[2]

[1]Institut de Science et d'Ingénierie Supramoléculaires (ISIS) CNRS UMR 7006, Université de Strasbourg, 8 Allée Gaspard Monge, 67000 Strasbourg, France

[2]Ecole Nationale Supérieure de Chimie de Paris, Université PSL, CNRS, i-CLeHS, 75005 Paris, France

[3]Department of Chemistry and Biomolecular Sciences, University of Ottawa, Ottawa, Ontario, K1N 6N5, Canada

Correspondence

Corresponding authors: Joseph Moran and Thijs Stuyver.

Email: moran@unistra.fr

Email: thijs.stuyver@chimieparistech.psl.eu

Funding Information

This research was supported by the Interdisciplinary Thematic Institute ITI-CSC via the IdEx Unistra (ANR-10-IDEX- 0002) within the program Investissement d'Avenir. MP thanks the CSC Graduate School, funded by the French National Research Agency (CSC-IGS ANR-17-EURE-0016). This research was undertaken, in part, thanks to funding from the Canada Research Chairs Program. JEAR and TS acknowledge the French National Agency for Research (ANR) for a CPJ grant (ANR-22-CPJ1-0093-01). This work was granted access to the HPC resources of IDRIS under the allocation *2023-100732* granted by GENCI as well as HPC cluster of the University of Strasbourg under the allocation *g2024a239c*.

Abstract

Aqueous microdroplets have been reported to dramatically increase the rate of chemical reactions. Proposed mechanisms for this acceleration include confinement effects upon droplet evaporation, and Brønsted acid or electric field catalysis at the air-water interface. However, computational investigations indicate that the operation of these mechanisms is reaction-dependent, with conclusive evidence for a role for electric field catalysis still lacking. Here, we present a computational investigation of the reported abiotic phosphorylation of ribose and the subsequent formation of ribonucleosides, focusing on acidity and oriented external electric field (OEEF) effects. The most plausible reaction mechanism identified involves the protonation of ribose, followed by carbocation formation and an S_N2 substitution step. Without an OEEF, all considered pathways are thermally inaccessible. However, in the presence of a significant OEEF, the S_N2-based pathway, leading to the β-ribonucleoside isomer, becomes highly stabilized, reducing the energetic span to a thermally accessible 12-13 kcal/mol. Surprisingly, the OEEF-mediated reaction closely mirrors the enzymatic mechanism of phosphorolysis via S_N2 substitution, including a pronounced anomeric selectivity. Our results support the hypothesis that some reactions in aqueous microdroplets are accelerated by electric fields and provide further evidence for the importance of electrostatic catalysis in biological systems, particularly for phosphorylase enzymes.

KEYWORDS

aqueous microdroplets, electric field catalysis, abiotic, mechanism

1 | INTRODUCTION

The physicochemical environment of aqueous microdroplets is distinct from bulk water, which can be exploited to accelerate reactions or even enable otherwise unfeasible transformations.[1,2,3,4,5,6,7] Recent examples of microdroplet-catalyzed transformations include the acceleration of the Menshutkin,[8,9] Diels-Alder,[10,11,12], and Aza-Michael reactions,[13] as well as CO_2 reduction to formic acid.[14,15]

Deciphering the factors that are responsible for the intriguing catalytic effect observed is a nontrivial task, in part due to the transient nature of microdroplets and because of their fairly small reaction volumes. At the same time, the size of microdroplets

Abbreviations: OEEF: oriented external electric field.

makes it unfeasible to simulate their full complexity *in silico*. Nevertheless, several hypotheses have been put forward over the years, ranging from partial solvation and solvent ordering, pH gradients, to the influence of electric fields.[16,17,18,3,1,19,20]

For instance, in a recent study, Song *et al.* argued that for the Aza-Michael addition reaction, enhanced acidity is the main accelerating factor, whereas the effect of a microdroplet's interfacial electric field is marginal at best.[13] Gong and co-workers on the other hand argued that neither electric fields nor partial solvation are responsible for Diels-Alder reaction acceleration,[12] but rather the confinement caused by microdroplet shrinking. Based on these conflicting findings, it appears that the catalytic mechanism seems to depend on the type of studied system, which implies that the effects exerted by the microdroplet environment should be examined in a case-by-case manner.

Recently, Zare and co-workers demonstrated that D-ribose can be phosphorylated to ribose-1-phosphate and subsequently transformed to uridine in the presence of phosphoric acid and uracil in aqueous microdroplets (cf. Figure 1).[21] The same conditions were shown to enable the formation of other sugar phosphates, as well as other purine and pyrimidine nucleosides.[22] The experimental conditions strongly suggest the assistance of oriented external electric fields (OEEFs), as the intrinsic electric field of aqueous microdroplets had to be complemented with an externally applied voltage to observe maximal catalysis.

In this computational study, we explore the mechanism of both reaction steps associated with the experiments performed by Zare and co-workers. Our calculations reveal that OEEFs indeed have a strong catalytic effect on both ribose phosphorylation and subsequent nucleoside formation. Interestingly, the key aspects of the uncovered mechanism, as well as the inferred anomeric selectivity, are in close resemblance to the enzymatic mechanism of phosphorolysis performed by purine or pyrimidine nucleoside phosphorylases[23,24] confirming that OEEFs also ought to play an important role in enzymatic catalysis.[25]

On the methodological side, we demonstrate that strong electric fields can radically reshuffle the conformer stability order of flexible molecules, such as ribose and its derivatives. As such, a rigorous treatment of conformational space, both in the presence and absence of electric fields, is essential to ensure the selection of representative conformers, and hence the construction of meaningful reaction profiles.

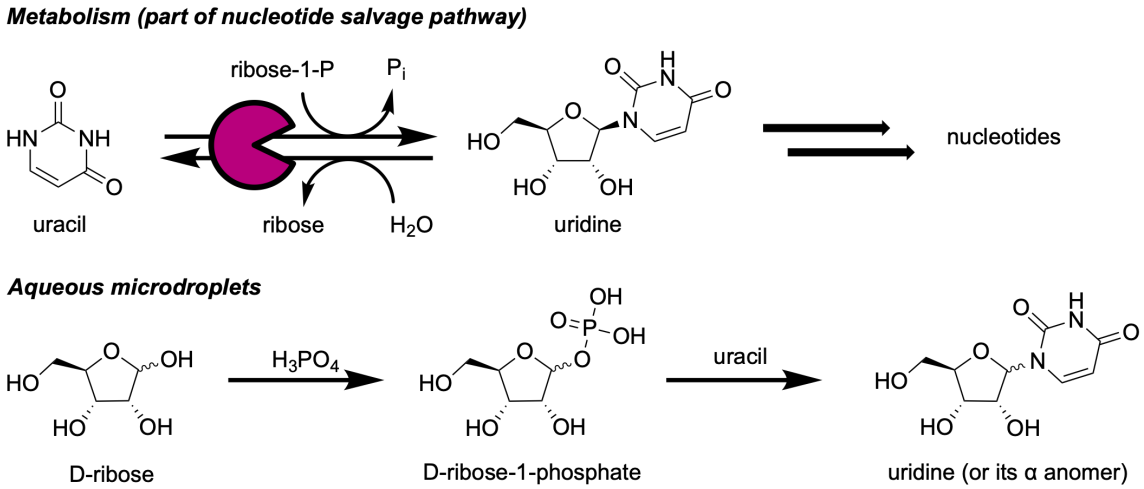

FIGURE 1 Uridine formation as part of the nucleotide salvage pathway in biochemistry is catalyzed by purine nucleoside phosphatase (top). Zare *et al.* showed that D-ribose can be phosphorylated selectively to ribose-1-phosphate by phosphoric acid and can subsequently be transformed into uracil in aqueous microdroplets (bottom).[21]

2 | METHODOLOGY

Initial geometries of the stationary points along the reaction profiles have been determined with the help of either autodE[26] or TS-tools.[27] The reaction SMILES used can be found in Section S1.1 of the Supporting Information. For each of the identified stationary states, conformer searches were performed as a post-processing step at GFN2-xTB[28] level-of-theory with the help of

https://doi.org/10.26434/chemrxiv-2024-m39s3 **ORCID:** https://orcid.org/0000-0001-6616-8920

CREST.[29,30] During conformational searches of the transition states, geometric constraints were applied to the active bonds, i.e., the bonds undergoing a change in bonding situation throughout the reaction, to preserve the TS vibrational mode. The 100 conformers with the lowest xTB energy were re-optimized with DFT, and the resulting energies were used to perform a final conformer ranking; the lowest energy conformer was subsequently selected for further refinement.

As the level of theory for the DFT calculations, we selected M06-2X/def2-SVP[31,32] for optimizations and frequency calculations, i.e., thermal corrections. Single-point energy refinements were performed at M06-2X/def2-TZVPD[31,32,33] level of theory. All DFT calculations were performed using Gaussian16.[34] Water solvation effects were accounted for through the SMD implicit solvent model.[35] Free energy corrections were calculated at 298.15 K and 1 mol/l. Quasi-harmonic corrections to entropy and enthalpy were applied using GoodVibes.[36] Grimme's method for the entropy[37] and the Head-Gordon enthalpy correction were applied,[38] where the frequency cut-off was set to 100 cm^{-1}. CM5 charges[39] were computed for key species. The structures of all reactants, products, and pre-reactive complexes were confirmed as having only positive eigenvalues in their Hessian matrix, while transition state structures were confirmed to have a single negative eigenvalue. Intrinsic Reaction Coordinate (IRC) analysis[40] confirmed that the transition state correctly connects the reactant state to the corresponding product. Optimized structures were represented using CYLview 2.0.[41] and VMD[42].

The effect of OEEFs was studied using the "Field = M ± N" keyword, which defines the OEEF axis, direction, and magnitude in Gaussian16. A range of field strengths (F_z) was explored, ranging from F_z= -0.30 V $Å^{-1}$ to F_z= +0.30 V $Å^{-1}$, with intervals of 0.10 V $Å^{-1}$. This range covers the full range of electric field strength estimates in microdroplets in the literature.[3,1]

It should also be mentioned here that in the Gaussian16 software, the positive direction of OEEF is defined from the negative to the positive charge which is opposite to the conventional definition in physics. We primarily applied the electric fields along the dipole moment, $\boldsymbol{\mu}$, of the individual species (labeled the Z-axis of the system), since OEEFs have a "tweezer" effect on molecules in solution and/or in the gas phase (i.e., molecules reorient in the direction that maximally stabilizes their dipole moment).[43] As such, this orientation can be expected to be the most prevalent one taken on by the considered molecular systems under the influence of a uniform field.[44] In Figure 2, a schematic overview of the adopted field, dipole, and z-axis definition is provided.

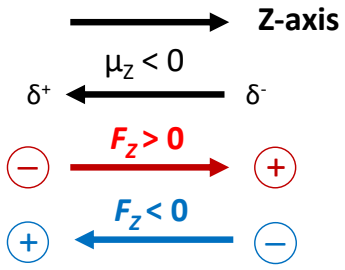

FIGURE 2 The Gaussian convention for electric fields, to which we adhered in this work.

When evaluating electric field effects, the 100 conformers obtained in the absence of a field were re-optimized, and subsequently re-ranked, in the presence of one, at DFT level of theory. As already indicated in the introduction, this rigorous – and computationally expensive – treatment of conformer space turned out to be essential in our analysis: for many species, we observed that the conformer ranking changes dramatically upon turning on the OEEF. Conformers that in the absence of a field don't even appear in the top 20 can all of a sudden become the lowest energy conformer when an electric field is taken into account (see Figure 3 for a representative example). As such, the traditional computational approach to evaluate electric field effects by focusing on the stabilization of the lowest energy conformer for every species identified along the reaction profile in the absence of an electric field would have induced significant errors in the presented results.

Finally, it should also be noted that to evaluate and compare the feasibility of individual reaction pathways, we make use here of the energetic span model, which posits that the rate at which a multistep reaction takes place can be deduced from the (free) energy difference between the lowest intermediate and the (subsequent) highest transition state along its profile.[45,46]

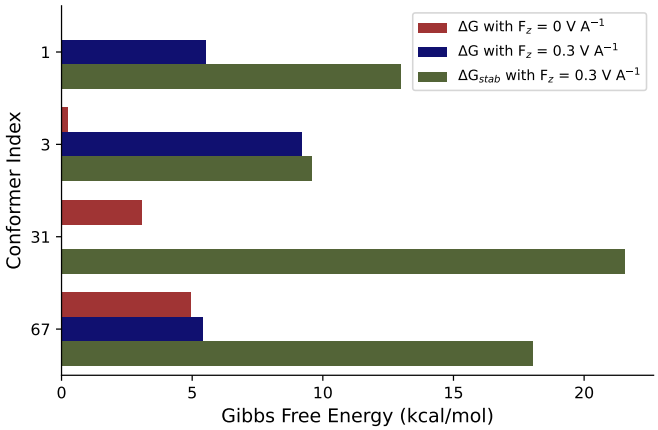

FIGURE 3 Effect of an OEEF with a field strength of 0.3 V Å^{-1} in four different conformers of α-ribose phosphate. The red and blue bars are the relative free energies with respect to the lowest energy conformer without the field and with a field strength of 0.3 V Å^{-1} respectively. The green bars represent the energetic stabilization (absolute values) under the influence of the OEEF. One can observe that both conformers 31 and 67 drop below conformer 1 in the presence of the electric field due to a disproportionate electrostatic stabilization.

3 | RESULTS AND DISCUSSION

In Figure 4, an overview of all the mechanistic pathways considered as part of this study is provided. Below, these pathways, and their feasibility to transpire in practice, will be discussed one by one.

3.1 | Phosphorylation of ribose

We started our mechanistic explorations from the biologically relevant form of ribose, i.e., the α-D-furanose form, and considered various possible pathways to prepare this species for eventual reaction with the uracil nucleobase. As such, we computed a variety of plausible concerted and stepwise mechanisms resulting in the installation of a phosphoric acid moiety on the ribose. Our calculations unequivocally indicate that for regular ribose, neither concerted, S_N2-like, nor stepwise phosphorylation pathways, proceeding via a pentavalent phosphorous intermediate, are feasible – typical reaction barriers amount to 40-60 kcal/mol, and electric fields aligned with the dipole moment of the reacting system only affect these barriers by a couple of kcal/mol at best (see Figure 6).

When applying the field along various directions in three dimensions it becomes apparent that the one coinciding with the dipole moment is associated with the strongest catalysis (Z-axis in Figure 5). It is however not the only field orientation leading to non-negligble barrier modulation. The orientation corresponding to the bond-breaking orientation also induces changes comparable to when the field is aligned with the dipole moment.

Note that our calculations recover the posited slight endothermicity of the neutral phosphorylation reaction, in close agreement with experimental estimates (2.7 kcal/mol computed for α-ribose in the field-free situation here, vs. the experimental value of 5.1 kcal/mol deduced from thermodynamic cycles), providing confidence in the accuracy of the selected level of theory.[47]

Overall, our calculations suggest that under standard bulk aqueous conditions, phosphorylation should not occur, in line with experimental observations.[48,21] In the microdroplet experiments performed by Zare and co-workers, however, H_3PO_4 is present in millimolar concentrations so that the reaction medium can be expected to be fairly acidic (pH $\sim$ 3)[21,22] – and that is even before any pH-altering interface effects are taken into account.[49] Under such reaction conditions, one can expect a non-negligible fraction of the ribose molecules to be protonated at any given time. In its protonated form, ribofuranose should dissociate fairly easily in a carbocation and water. This dissociation will be particularly favored if the carbocation is formed in the 1' position, since a resonance-stabilized oxocarbenium species is generated in this manner.

With the M06-2X functional, no TS could be located for this dissociation reaction. Interestingly, however, a barrier can readily be recovered when switching over to the M06 functional, as a shallow minimum – corresponding to a loose complex – is formed

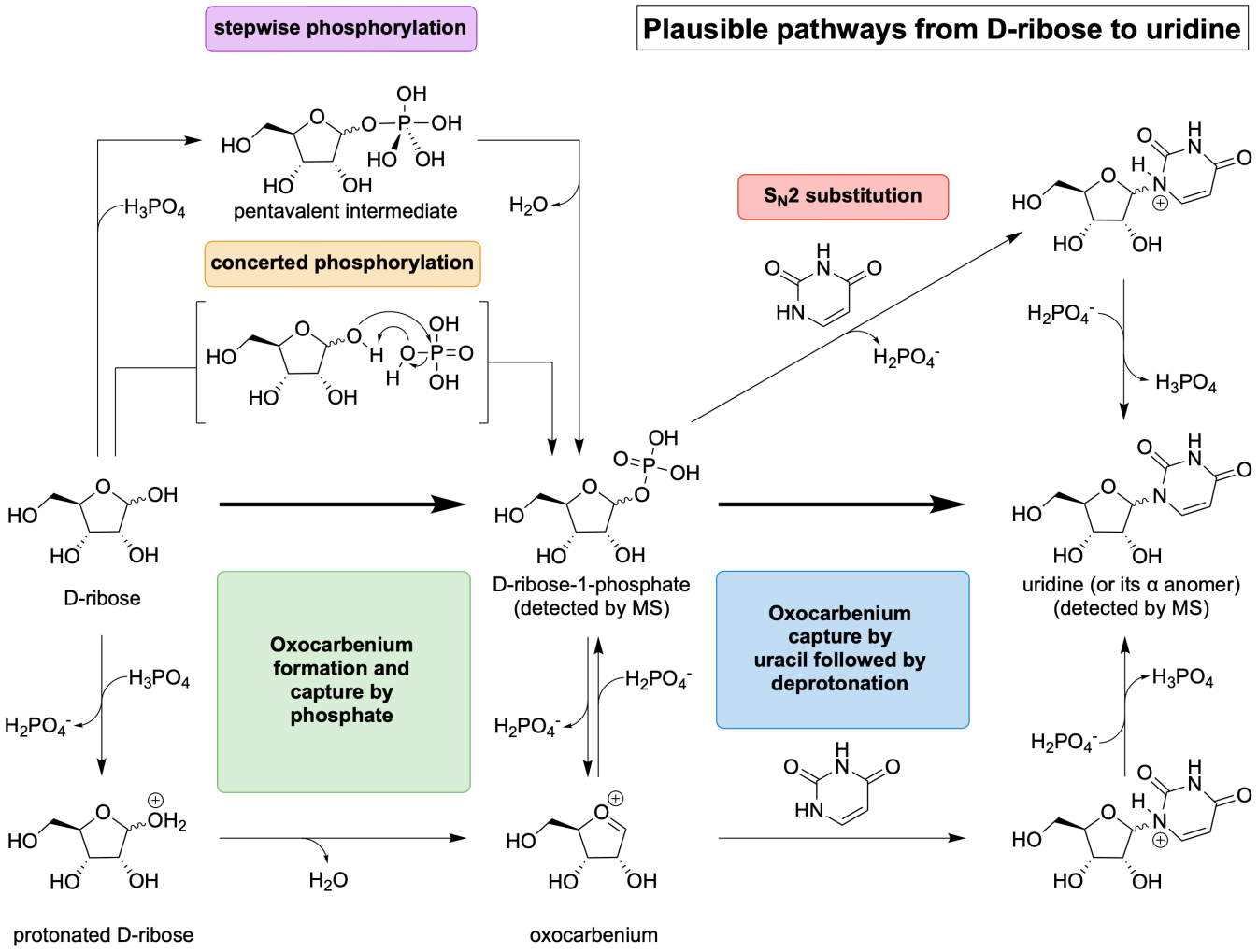

FIGURE 4 Plausible pathways for the phosphorylation of ribose and uracil formation from D-ribose and phosphoric acid in water.

at this level of theory. The computed M06 barrier amounts to 11 kcal/mol, which agrees with the approximate dissociation energy inferred from a relaxed scan along the C-O bond axis with the M06-2X functional (see Section S2 of the Supporting Information). As such, one can reasonably expect the carbocation to be thermally accessible in acidic solution (see Section S3 of the SI for a more in-depth discussion).

Turning to the effect of applying an OEEF, we observe that significant catalysis of the dissociation event is possible in principle: at an electric field strength of -0.1 V Å^{-1} aligned with the dipole moment, the approximate dissociation energy is reduced to about 9 kcal/mol, and at -0.3 V Å^{-1}, the dissociation becomes even more favorable: at no point along the relaxed scan performed does the relative (free) energy exceed 6 kcal/mol, and at full dissociation, the relative energy has returned to essentially zero (despite the apparent emergence of a barrier, we were unable to locate one explicitly).

It should however be noted that negative electric field strengths actually destabilize the protonated ribose, hence in the presence of the OEEF, molecular rotation ought to take place, resulting in a flip of the field direction. Since the considered dissociation would be the very first reaction step of the overall process, it may compete with rotation during microdroplet formation, especially since the former is an almost barrierless event. As such, a fraction of the ribose molecules likely dissociates in an electric field-mediated manner the very instant the microdroplets emerge.

At the same time, it should also be noted that even after the molecular rotation has been completed, dissociation of the protonated species is still most certainly feasible; even at a field strength of +0.3 V Å^{-1}, the approximate dissociation energy amounts to only 12 kcal/mol, i.e., a negligible inhibition compared to the field-free situation.

https://doi.org/10.26434/chemrxiv-2024-m39s3 **ORCID:** https://orcid.org/0000-0001-6616-8920

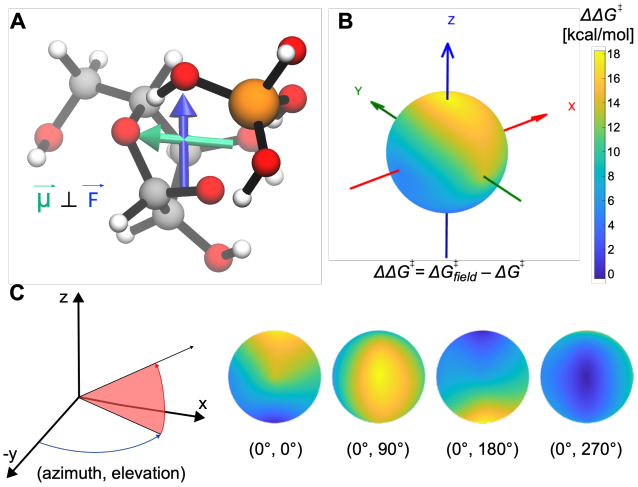

FIGURE 5 Assesing the optimal electric field orientation. A: In the transition state of the first step in the stepwise pathway of phosphorylation of α-ribose by H_3PO_4 the O-P bond forming axis is almost perpendicular to the dipole moment aligned with the z-axis. B: The difference between the free energy of the transition state with and without the applied OEEF ($\Delta\Delta G^{\ddagger}$) as a function of the field's orientation in space visualized on a spheric surface. C: Rotated views of the sphere are provided on the right side of the figure, with the rotation coordinates expressed in terms of azimuth and elevation angles (angle of rotation around the z-axis and the angle between the projection point and xy plane, respectively).

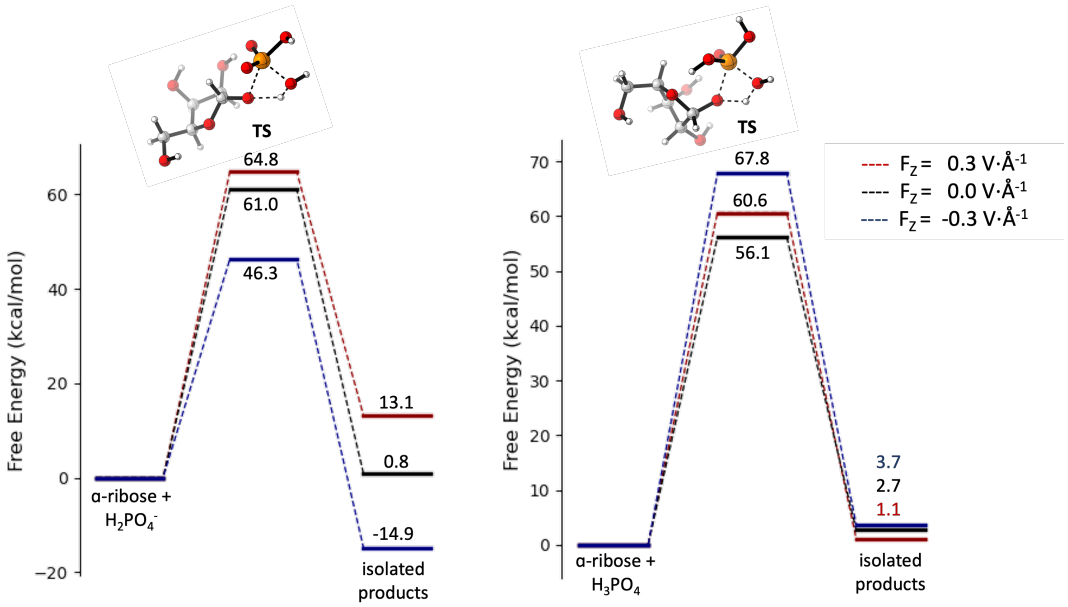

FIGURE 6 The identified concerted phosphorylation pathways without an OEEF (black) and with an OEEF of magnitude $\pm$ 0.3 V Å^{-1} applied in the direction of the dipole moment (red and blue profiles, respectively).

Finally, at a pH of around 3, the most prevalent form of phosphoric acid is $H_2PO_4^-$ (the pKa of the first deprotonation event of this species amounts to 2.14).[50] This species readily associates with the formed oxocarbenium in a barrierless process that is exergonic by 22.3 kcal/mol. During this step, the α and β isomers are resolved thermodynamically, and the β ribofuranose-phosphoric acid is most stable by 4.1 kcal/mol.

https://doi.org/10.26434/chemrxiv-2024-m39s3 **ORCID:** https://orcid.org/0000-0001-6616-8920

Taking everything together, our calculations thus provide unequivocal computational support for the observed spontaneous phosphorylation of ribose in microdroplets, and it is clear that this transformation is promoted by a synergy between (enhanced) acidity and electric field effects.

3.2 | Formation of the ribonucleoside from the phosphorylated ribose

For the formation of the final ribonucleoside, starting from ribofuranose-phosphoric acid, various pathways can be conceived as well; we focus first on the S_N1 and S_N2 substitution ones in our analysis below.

In the absence of an electric field, the activation energy for the S_N2 is unrealistically high; 36.8 kcal/mol for the α isomer and 39.9 kcal/mol for the β isomer (Figure 7). Note that this is even the case when the phosphoric acid moiety is fully protonated (a necessary condition for it to become a good leaving group). It should be noted that the TS for this reaction pathway is in fact a loose complex with a distance between the leaving group and the substrate of around 2.9 Å; this kind of complex has also been found in other reactions involving sugars.[51]

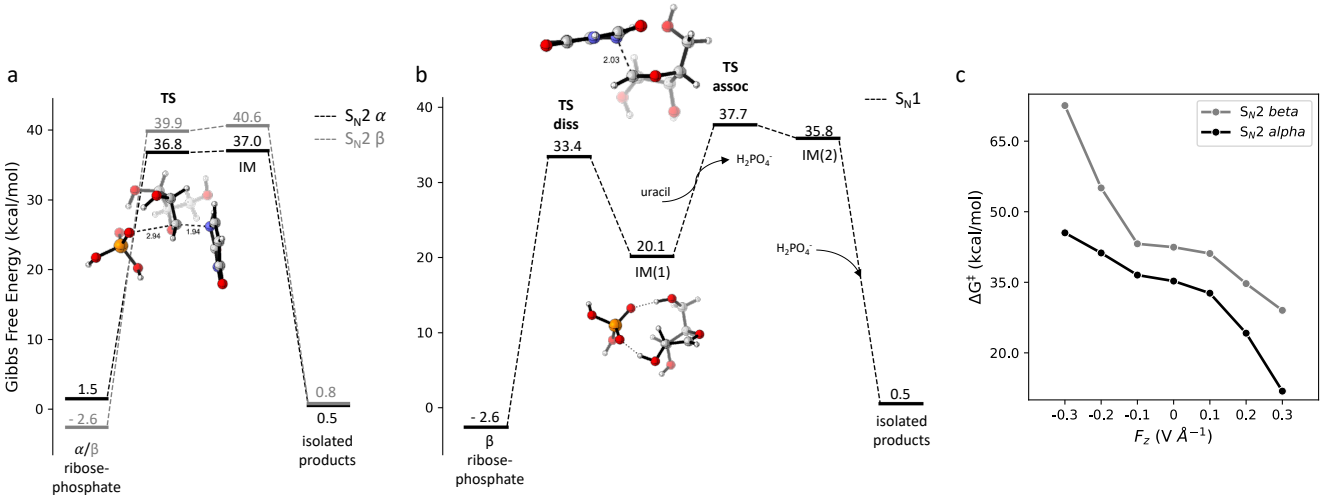

FIGURE 7 M06-2X/def2-TZVPD//M06-2X/def2-SVP free energy profile for the a) S_N2 mechanism in water of α-ribofuranosyl phosphate and β-ribofuranosyl phosphate, b) S_N1 mechanism in water of β-ribofuranosyl phosphate. c) $\Delta G^{\ddagger}$ values of transition states for S_N2 pathway as a function of field strength F_z. TS = transition state, IM = Intermediate.

Our calculations indicate that electric fields oriented along the dipole moment of the reacting system have a dramatic effect on the kinetics of this pathway. Remarkably, it is especially the TS involving the α isomer that is extremely susceptible to electrostatic stabilization: at 0.1 V Å^{-1}, the reaction barrier is already reduced by around 4 kcal/mol, at 0.3 V Å^{-1}, the barrier reduction amounts to a staggering 26 kcal/mol, i.e., the barrier for the elementary step starting from ribose phosphate has reduced to a mere 11 kcal/mol. For the β isomer, our calculations suggest that the potential for electrostatic catalysis is much more subdued; only 10 kcal/mol of barrier reduction is obtained at the highest OEEF strength probed (cf. Figure 7c).

It should be noted that at high OEEF magnitudes, the S_N2 pathway becomes increasingly asynchronous, with the phosphate seemingly detached from the ribose in the TS structure. Nevertheless, full dissociation does not take place even at the highest electric field strength probed. Importantly, the increasing separation between the leaving group and the ribose, in combination with the persistent (partial) intramolecular charge transfer of 0.1e, causes the emergence of a huge dipole moment of 49 D, which, in the case of the reaction starting from the α isomer, in particular, is almost perfectly aligned with the reaction axis. It is this growing dipole moment that is responsible for the remarkable catalysis observed for this species.

For the S_N1 pathway, the activation energy is of the same order as for the S_N2 pathway in the absence of an electric field; the barrier of the rate-determining reaction step amounts to 37.7 kcal/mol. In the presence of an OEEF aligned with the dipole moment, however, no significant catalysis is observed. The reason for this limited effect is that now, the reaction axis associated

with the second TS is orthogonal to the dipole moment (see Section S6 of Supporting Information). As such, the rate-determining TS is not stabilized significantly, whereas the reactant, i.e., the ribofuranosyl phosphate species, is.

A final pathway that could potentially be envisioned is direct oxocarbenium capture by uracil, followed by deprotonation. In essence, this corresponds to the S_N1 pathway, but without the initial ribose-phosphate dissociation. As our calculations indicate that the rate-determining step of the S_N1 pathway is retained in this final alternative, both are equally unlikely to transpire: the energetic spans, as well as the susceptibility to electric field effects, are the same.

3.3 | Evaluation of the full reaction profile

Overall, it should be clear that the only feasible reaction pathway leading to the ribonucleoside emerging from our computations is the S_N2 pathway, involving α-ribofuranosyl phosphate. The overall energetic span of the protonation – dissociation – S_N2 pathway, starting from the original, protonated ribose, effectively amounts to a mere 12-13 kcal/mol with an electric field strength of ± 0.3 V Å^{-1} in the worst case situation (cf. Fig. 8), suggesting reaction rates that would easily result in detectable concentrations of the experimentally observed ribonucleoside on the typical timescale of microdroplet experiments (100s of μs up to a couple of ms).[21]

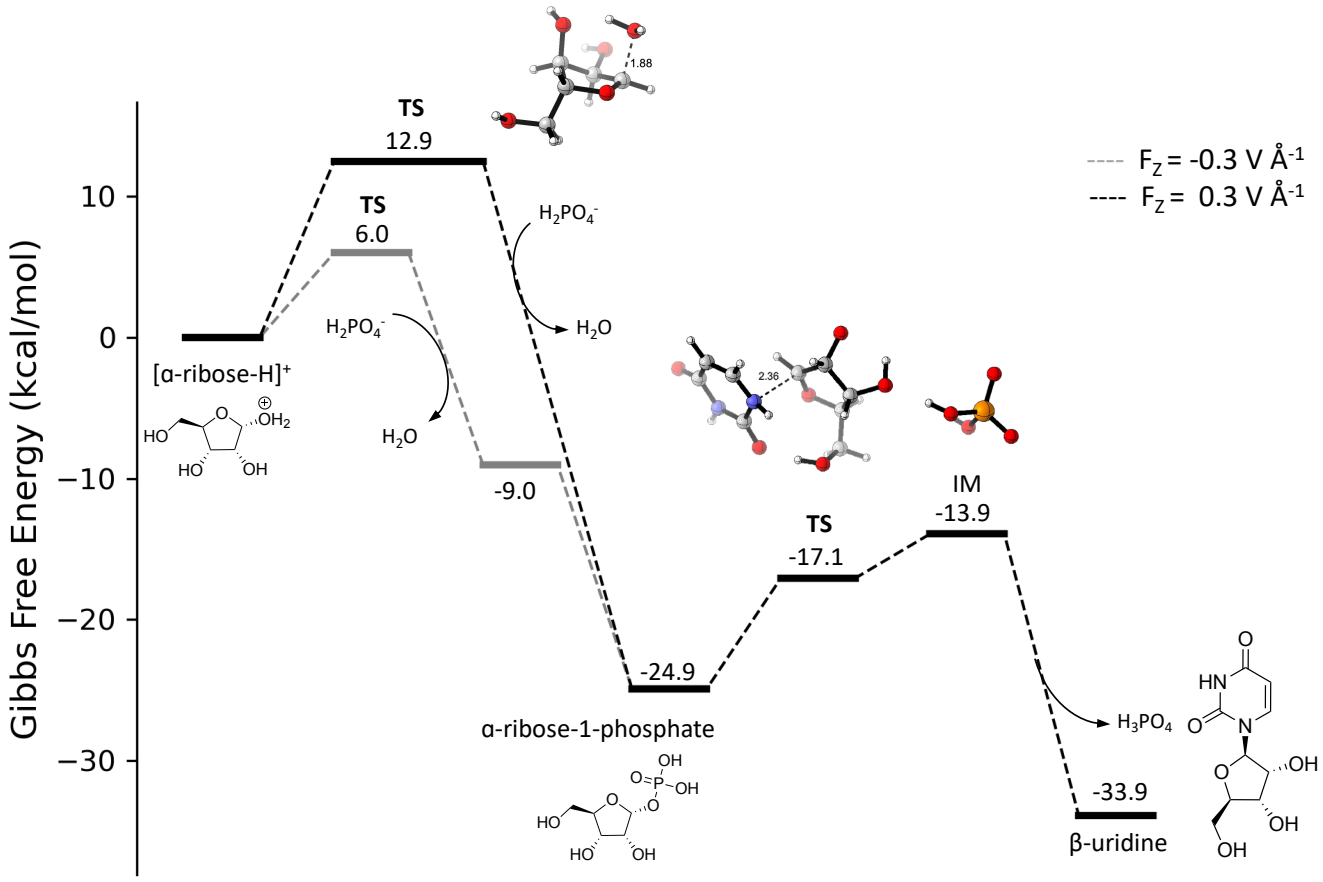

FIGURE 8 M06-2X/def2-TZVPD//M06-2X/def2-SVP free energy profile for the conversion of protonated α-ribose into β-uridine under the effect of a field with $F_z = \pm 0.3$ V A^{-1}. TS = transition state, IM = Intermediate

It is important to underscore at this point that a significant amount of uncertainty remains: as already discussed in the introduction, the physics of microdroplets, and the precise impact of this peculiar environment on the chemistry taking place inside them, is not yet fully understood.[16,17,18,3,1,19,20] For example, the actual magnitude of the (intrinsic) electric field in

https://doi.org/10.26434/chemrxiv-2024-m39s3 **ORCID:** https://orcid.org/0000-0001-6616-8920

microdroplets has been debated extensively, and diverging estimates have been put forward.[3,1,19,20] 0.3 V Å^{-1} clearly falls near the upper limit of what may be considered as realistic, and our calculations indicate that at significantly lower field strengths, the S_N2 pathway quickly becomes less favorable. However, as recently pointed out by Head-Gordon and co-workers, all estimates provided so far focused on the *average* electric field magnitude near the surface of microdroplets. In practice, fluctuations at the microdroplet interface likely result in a Lorentzian spread of field values,[52] implying that 0.3 V Å^{-1} may be achieved locally, and momentarily, even if the average field strength would turn out to be significantly lower. Regardless of this point of uncertainty, it should be clear that the mechanism proposed above is the only plausible option among the ones considered in this study, as every other possibility involves an energetic span that is at least 20-25 kcal/mol bigger (even in the presence of extreme electric field strengths), thus exceeding by far the window of reactions feasible at room temperature on a (mili)second scale.

It is also important to note that in principle, the validity of our calculations could easily be confirmed – or falsified – experimentally. As indicated above, our results suggest that there should be a clear preference in the stereochemistry of the ribonucleoside formed in microdroplets, with the β isomer being preferred over the α one by a significant margin. In the experiments by Zare and co-workers, the stereochemistry of the formed products was not characterized,[21,22] but if upon replication, it would be observed that only a single stereoisomer would be formed, then that would provide unequivocal support for the mechanism, involving an S_N2 elementary step, described above.

4 | CONCLUSIONS

Here, we have computationally investigated the mechanism of abiotic phosphorylation of ribose, and the subsequent formation of ribonucleosides. Various mechanistic possibilities were considered, with a particular focus on the effect of acidity and electric field effects. Our calculations suggest that the most plausible reaction pathway involves protonation of the starting compound ribose, followed by carbocation formation through dissociation, and finally an S_N2 reaction step. In the absence of an external electric field, this reaction pathway, as well as all the other reaction pathways considered, involve energetic spans exceeding 30-40 kcal/mol, so they won't take place in practice. When a significant OEEF is applied, however, the S_N2-based pathway – resulting in the β isomer – is stabilized remarkably (the energetic span reduces to 11 kcal/mol), and hence becomes thermally accessible. Since the other reaction pathways considered are much less susceptible to electric field effects, one can conclude that the described protonation – dissociation – S_N2 pathway is the only plausible one in microdroplets – under the assumption that significant electric fields are indeed present in these environments. Since our calculations suggest that the proposed mechanism involves a strong anomeric preference, straightforward experimental verification is in principle possible.

Notably, the presented mechanism strongly resembles the enzymatic mechanism of phosphorolysis, both in terms of the actual reaction pathway taken (S_N2), and the observed selectivity. This finding underscores that the catalysis exerted by phosphorylase enzymes is also likely caused by (local) electric fields surrounding the active site, in line with the electrostatic catalysis hypothesis originally proposed by Warshel and co-workers.[25]

5 | DATA AVAILABILITY

The log files for all calculations can be downloaded from Figshare at https://figshare.com/projects/Abiotic_ribonucleoside_formation_in_microdroplets_mechanistic_exploration_acidity_and_electric_field_effects/223206.

AUTHOR CONTRIBUTIONS

MP: software, methodology, formal analysis, visualization, writing. JEAR: software, methodology, formal analysis, visualization, writing. TS: conceptualization, methodology, formal analysis, writing, supervision, funding acquisition. JM: conceptualization, methodology, formal analysis, writing, supervision, funding acquisition.

REFERENCES

1. Hao H, Leven I, Head-Gordon T. Can electric fields drive chemistry for an aqueous microdroplet?. *Nat. Commun.*. 2022;13(1):280.
2. Shaik S, Danovich D, Joy J, Wang Z, Stuyver T. Electric-field mediated chemistry: uncovering and exploiting the potential of (oriented) electric fields to exert chemical catalysis and reaction control. *J. Am. Chem. Soc.*. 2020;142(29):12551–12562.

3. Xiong H, Lee JK, Zare RN, Min W. Strong electric field observed at the interface of aqueous microdroplets. *J. Phys. Chem. Lett.*. 2020;11(17):7423–7428.
4. Zhao L, Song X, Gong C, et al. Sprayed water microdroplets containing dissolved pyridine spontaneously generate pyridyl anions. *Proc. Natl. Acad. Sci.*. 2022;119(12):e2200991119.
5. Jin S, Chen H, Yuan X, et al. The spontaneous electron-mediated redox processes on sprayed water microdroplets. *J. Am. Chem. Soc. Au.* 2023;3(6):1563–1571.
6. Zhu C, Pham LN, Yuan X, Ouyang H, Coote ML, Zhang X. High electric fields on water microdroplets catalyze spontaneous and fast reactions in halogen-bond complexes. *J. Am. Chem. Soc.*. 2023;145(39):21207–21212.
7. Musskopf NH, Gallo Jr A, Zhang P, Petry J, Mishra H. The air–water interface of water microdroplets formed by ultrasonication or condensation does not produce h2o2. *J. Phys. Chem. Lett.*. 2021;12(46):11422–11429.
8. Tang C, Su M, Lu T, et al. Massive acceleration of SN 2 reaction using the oriented external electric field. *Chem. Sci.*. 2024;15(33):13486–13494.
9. Song Z, Liang C, Gong K, et al. Harnessing the high interfacial electric fields on water microdroplets to accelerate Menshutkin reactions. *J. Am. Chem. Soc.*. 2023;145(48):26003–26008.
10. Aragones AC, Haworth NL, Darwish N, et al. Electrostatic catalysis of a Diels–Alder reaction. *Nature.* 2016;531(7592):88–91.
11. Meir R, Chen H, Lai W, Shaik S. Oriented electric fields accelerate Diels–Alder reactions and control the endo/exo selectivity. *ChemPhysChem.* 2010;11(1):301–310.
12. Gong K, Nandy A, Song Z, et al. Putting Enhanced Chemical Reactivity in Water Microdroplets Under the Microscope: The Case of a Diels-Alder Reaction. *ChemRxiv.* 2024.
13. Song Z, Zhu C, Gong K, et al. Deciphering the Microdroplet Acceleration Factors of Aza-Michael Addition Reactions. *J. Am. Chem. Soc.*. 2024;146(15):10963–10972.
14. Song X, Meng Y, Zare RN. Spraying water microdroplets containing 1, 2, 3-triazole converts carbon dioxide into formic acid. *J. Am. Chem. Soc.*. 2022;144(37):16744–16748.
15. Gong K, Meng Y, Zare RN, Xie J. Molecular Mechanism for Converting Carbon Dioxide Surrounding Water Microdroplets Containing 1, 2, 3-Triazole to Formic Acid. *J. Am. Chem. Soc.*. 2024;146(12):8576–8584.
16. Mishra H, Enami S, Nielsen RJ, et al. Brønsted basicity of the air–water interface. *Proc. Natl. Acad. Sci.*. 2012;109(46):18679–18683.
17. Wei H, Vejerano EP, Leng W, et al. Aerosol microdroplets exhibit a stable pH gradient. *Proc. Natl. Acad. Sci.*. 2018;115(28):7272–7277.
18. Gong K, Ao J, Li K, et al. Imaging of pH distribution inside individual microdroplet by stimulated Raman microscopy. *Proc. Natl. Acad. Sci.*. 2023;120(20):e2219588120.
19. Chamberlayne CF, Zare RN. Simple model for the electric field and spatial distribution of ions in a microdroplet. *J. Chem. Phys.*. 2020;152(18):184702.
20. Ju Y, Zhang H, Jiang Y, et al. Aqueous microdroplets promote C–C bond formation and sequences in the reverse tricarboxylic acid cycle. *Nat. Ecol. Evol.*. 2023;7(11):1892–1902.
21. Nam I, Lee JK, Nam HG, Zare RN. Abiotic production of sugar phosphates and uridine ribonucleoside in aqueous microdroplets. *Proc. Natl. Acad. Sci.*. 2017;114(47):12396–12400.
22. Nam I, Nam HG, Zare RN. Abiotic synthesis of purine and pyrimidine ribonucleosides in aqueous microdroplets. *Proc. Natl. Acad. Sci.*. 2018;115(1):36–40.
23. Erion MD, Stoeckler JD, Guida WC, Walter RL, Ealick SE. Purine nucleoside phosphorylase. 2. Catalytic mechanism. *Biochemistry.* 1997;36(39):11735–11748.
24. Isaksen GV, Hopmann KH, Åqvist J, Brandsdal BO. Computer simulations reveal substrate specificity of glycosidic bond cleavage in native and mutant human purine nucleoside phosphorylase. *Biochemistry.* 2016;55(14):2153–2162.
25. Warshel A. Electrostatic origin of the catalytic power of enzymes and the role of preorganized active sites. *J. Biol. Chem.*. 1998;273(42):27035–27038.
26. Young TA, Silcock JJ, Sterling AJ, Duarte F. autodE: automated calculation of reaction energy profiles—application to organic and organometallic reactions. *Angew. Chem., Int. Ed.*. 2021;133(8):4312–4320.
27. Stuyver T. TS-tools: Rapid and automated localization of transition states based on a textual reaction SMILES input. *J. Comput. Chem.*. 2024;45(27):2308–2317.
28. Bannwarth C, Ehlert S, Grimme S. GFN2-xTB—An accurate and broadly parametrized self-consistent tight-binding quantum chemical method with multipole electrostatics and density-dependent dispersion contributions. *J. Chem. Theory Comput.*. 2019;15(3):1652–1671.
29. Pracht P, Bohle F, Grimme S. Automated exploration of the low-energy chemical space with fast quantum chemical methods. *Phys. Chem. Chem. Phys.*. 2020;22(14):7169–7192.
30. Pracht P, Grimme S, Bannwarth C, et al. CREST—A program for the exploration of low-energy molecular chemical space. *J. Chem. Phys.*. 2024;160(11):114110.
31. Zhao Y, Truhlar DG. The M06 suite of density functionals for main group thermochemistry, thermochemical kinetics, noncovalent interactions, excited states, and transition elements: two new functionals and systematic testing of four M06-class functionals and 12 other functionals. *Theor. Chem. Acc.*. 2008;120:215–241.
32. Weigend F, Ahlrichs R. Balanced basis sets of split valence, triple zeta valence and quadruple zeta valence quality for H to Rn: Design and assessment of accuracy. *Phys. Chem. Chem. Phys.*. 2005;7:3297-3305.
33. Pritchard BP, Altarawy D, Didier B, Gibson TD, Windus TL. New Basis Set Exchange: An Open, Up-to-Date Resource for the Molecular Sciences Community. *J. Chem. Inf. Model.*. 2019;59(11):4814–4820.
34. Frisch MJ, Trucks GW, Schlegel HB, et al. Gaussian~16 Revision C.01. https://gaussian.com/gaussian16/; 2016. Gaussian Inc. Wallingford CT.
35. Marenich AV, Cramer CJ, Truhlar DG. Universal solvation model based on solute electron density and on a continuum model of the solvent defined by the bulk dielectric constant and atomic surface tensions. *J. Phys. Chem. C.* 2009;113(18):6378–6396.
36. Luchini G, Alegre-Requena JV, Funes-Ardoiz I, Paton RS. GoodVibes: automated thermochemistry for heterogeneous computational chemistry data. *F1000Research.* 2020;9(291):291.
37. Grimme S. Supramolecular binding thermodynamics by dispersion-corrected density functional theory. *Chem. A Eur. J.*. 2012;18(32):9955–9964.
38. Li YP, Gomes J, Mallikarjun Sharada S, Bell AT, Head-Gordon M. Improved force-field parameters for QM/MM simulations of the energies of adsorption for molecules in zeolites and a free rotor correction to the rigid rotor harmonic oscillator model for adsorption enthalpies. *J. Phys.*

Chem. C. 2015;119(4):1840–1850.
39. Marenich AV, Jerome SV, Cramer CJ, Truhlar DG. Charge Model 5: An Extension of Hirshfeld Population Analysis for the Accurate Description of Molecular Interactions in Gaseous and Condensed Phases. *J. Chem. Theory Comput.*. 2012;8(2):527-541.
40. Fukui K. The path of chemical reactions-the IRC approach. *Acc. Chem. Res.*. 1981;14(12):363–368.
41. Legault CY. CYLview20; Legault, C. Y., Université de Sherbrooke, 2020 (http://www.cylview.org). http://www.cylview.org; .
42. Humphrey W, Dalke A, Schulten K. VMD: visual molecular dynamics. *Journal of molecular graphics.* 1996;14(1):33–38.
43. Wang C, Danovich D, Chen H, Shaik S. Oriented external electric fields: Tweezers and catalysts for reactivity in halogen-bond complexes. *J. Am. Chem. Soc.*. 2019;141(17):7122–7136.
44. Dutta Dubey K, Stuyver T, Kalita S, Shaik S. Solvent organization and rate regulation of a menshutkin reaction by oriented external electric fields are revealed by combined MD and QM/MM calculations. *J. Am. Chem. Soc.*. 2020;142(22):9955–9965.
45. Kozuch S, Shaik S. How to conceptualize catalytic cycles? The energetic span model. *Acc. Chem. Res.*. 2011;44(2):101–110.
46. Kozuch S. A refinement of everyday thinking: the energetic span model for kinetic assessment of catalytic cycles. *Wiley Interdiscip. Rev.: Comput. Mol. Sci.*. 2012;2(5):795–815.
47. Camici M, Sgarrella F, Ipata PL, Mura U. The standard gibbs free energy change of hydrolysis of α-d-ribose 1-phosphate. *Arch. Biochem. Biophys.*. 1980;205(1):191–197.
48. Fuller WD, Sanchez RA, Orgel LE. Studies in prebiotic synthesis: VI. Synthesis of purine nucleosides. *Journal of molecular biology.* 1972;67(1):25–33.
49. Puente d. lM, Laage D. How the acidity of water droplets and films is controlled by the air–water interface. *J. Am. Chem. Soc.*. 2023;145(46):25186–25194.
50. O'Neil MJ, Heckelman PE, Koch CB, Roman KJ., eds.*The Merck Index: An Encyclopedia of Chemicals, Drugs and Biologicals*. Merck & Co, 1996.
51. Chan J, Sannikova N, Tang A, Bennet AJ. Transition-State Structure for the Quintessential SN2 Reaction of a Carbohydrate: Reaction of α-Glucopyranosyl Fluoride with Azide Ion in Water. *J. Am. Chem. Soc.*. 2014;136(35):12225-12228.
52. LaCour RA, Heindel JP, Zhao R, Head-Gordon T. The Role of Interfaces and Charge for Chemical Reactivity in Microdroplets. *arXiv.* 2024.